Dynamic Model for Metal Cleanness Evaluation by Melting in a Cold Crucible

V. BOJAREVICS, K. PERICLEOUS, and R. BROOKS

Melting of metallic samples in a cold crucible causes inclusions to concentrate on the surface owing to the action of the electromagnetic force in the skin layer. This process is dynamic, involving the melting stage, then quasi-stationary particle separation, and finally the solidification in the cold crucible. The proposed modeling technique is based on the pseudospectral solution method for coupled turbulent fluid flow, thermal and electromagnetic fields within the time varying fluid volume contained by the free surface, and partially the solid crucible wall. The model uses two methods for particle tracking: (1) a direct Lagrangian particle path computation and (2) a drifting concentration model. Lagrangian tracking is implemented for arbitrary unsteady flow. A specific numerical time integration scheme is implemented using implicit advancement that permits relatively large time-steps in the Lagrangian model. The drifting concentration model is based on a local equilibrium drift velocity assumption. Both methods are compared and demonstrated to give qualitatively similar results for stationary flow situations. The particular results presented are obtained for iron alloys. Small size particles of the order of 1 μm are shown to be less prone to separation by electromagnetic field action. In contrast, larger particles, 10 to 100 μm, are easily "trapped" by the electromagnetic field and stay on the sample surface at predetermined locations depending on their size and properties. The model allows optimization for melting power, geometry, and solidification rate.

DOI: 10.1007/s11663-009-9226-2

I. INTRODUCTION

METAL users are asking for increasingly clean alloys to avoid mechanical failure of components due to microstructural defects caused by oxide inclusions. Work has shown that by concentrating inclusions on the surface of a sample button by melting, either by cold crucible levitation melting or by other clean melting techniques, any small population of large, detrimental inclusions can be observed and analyzed far more effectively than using more traditional metallographic examination methods.[1] Cold crucible melting may also be used for element separation and concentration, for instance, in treating the nuclear fusion products generated after reprocessing of spent fuel.[2] Growing demands on metal cleanness and impurity control by size require a rapid analysis technique to determine the content of impurities in samples. Melting of small samples in the presence of an electromagnetic field can help to concentrate inclusions in specific positions on the surface. Barnard *et al.*[1] demonstrated experimentally that melting in a cold crucible with a high-frequency AC field indeed brings particles to selected locations on the surface of consequently solidified metallic sample. Taniguchi and Kikuchi[3] obtained material with a nonconducting additive collected near the surface of a cylindrical shaft and proposed a theory for the particle concentration variation in the presence of the imposed electromagnetic field and steady melt flow. Toh *et al.*[4,5] repeated the cold crucible experiments and attempted to predict numerically the particle paths in a computed steady flow. They used the electromagnetic force expression derived by Leenov and Kolin[6] for the forces acting on particles of varying electrical conductivity in constant crossed electric and magnetic fields. Experimental observations of the particles of various shapes and electrical conductivities in the liquid metal carrying electrical current are described in Reference 7. An expression similar to Leenov and Kolin's[6] was derived, but for the conditions of gradient magnetic field, which results in the increase of the effective force on the particles.[7]

The process of sample melting in a cold crucible is dynamic, involving the melting stage, then quasi-stationary particle separation, and finally the solidification in the crucible. The final distribution of the initially uniformly distributed particles of various sizes and properties needs to be assessed. The proposed modeling technique is based on the pseudo-spectral solution method for the coupled turbulent fluid flow, thermal and electromagnetic fields within the time varying fluid volume contained by the free surface, and partially the solid crucible wall.[8] The unsteady model for particle tracking is implemented using two methods: (1) a direct Lagrangian particle path computation[9,10] and a drifting

V. BOJAREVICS, Reader, and K. PERICLEOUS, Professor, are with the Centre for Numerical Modelling and Process Analysis, University of Greenwich, Park Row, London SE10 9LS, United Kingdom. Contact e-mail: v.bojarevics@gre.ac.uk R. BROOKS, Group Leader of Advanced Engineered Materials, is with the National Physical Laboratory, Teddington, Middlesex TW11 0LW, United Kingdom.

This article is based on a presentation given at the International Symposium on Liquid Metal Processing and Casting (LMPC 2007), which occurred in September 2007 in Nancy, France.

Article published online March 4, 2009.

concentration model.[11] Lagrangian tracking is implemented for arbitrary unsteady flow, which requires a specific numerical time integration scheme using implicit advancement in order to avoid severe stability restrictions. The drifting concentration model, which is based on a local equilibrium drift velocity assumption, is applied to the time varying concentration in a steady mean flow. Both methods give qualitatively similar results for stationary flow situations. The Lagrangian particle tracking is preferable for the unsteady processes. The final stage of dynamic solidification is expected to be of importance to determine particle location changes for laboratory analysis.

II. MATHEMATICAL MODELS

The mathematical and numerical modeling for the time-dependent fluid flow in a variable shape volume in axisymmetric approximation is described in previous publications.[8] The method is based on the continuous coordinate transformation adapting to the free surface and the containing vessel bottom. The present implementation accounts for the arbitrary shaped cold-crucible bottom. We will restrict the model description to the novel features of the particle tracking algorithm.

A. *Lagrangian Particle Tracking*

The position $\mathbf{R}(x,y,z,t)$ of an individual particle can be determined following its path and the variable total force $\mathbf{F}(x,y,z,t)$ acting on the particle by solving the set of two equations[8,9]:

$$\partial_t \mathbf{R} = \mathbf{u}_p \qquad [1]$$

$$m_p \partial_t \mathbf{u}_p = \mathbf{F} \qquad [2]$$

where $\mathbf{u}_p$ is the particle velocity and m_p its mass. The total force acting locally on the particle can be decomposed into the fluid drag force $\mathbf{F}_d$, the buoyancy force $\mathbf{F}_g$, and the effective electromagnetic force $\mathbf{F}_e$. The drag force depends on the Reynolds number:

$$\mathrm{Re}_p = \frac{d_p|\Delta\mathbf{u}|}{\nu} \qquad [3]$$

where d_p is the particle diameter, $\Delta\mathbf{u} = \mathbf{u} - \mathbf{u}_p$ is the (slip) velocity relative to the fluid velocity $\mathbf{u}$, and ν is the kinematic viscosity. For small particles, the Reynolds number Re_p is rather small, of the order O(1); therefore, the drag force can be approximated as

$$\mathbf{F}_d = \frac{3C_d^*\rho\pi d_p^2}{\mathrm{Re}_p}|\Delta\mathbf{u}|\Delta\mathbf{u} = 3C_d^*\nu\rho\pi d_p\Delta\mathbf{u}$$
$$C_d^* = 1 + 0.15\mathrm{Re}_p^{0.687} \quad (\mathrm{Re}_p < 1000) \qquad [4]$$

The buoyancy force due to the gravity $\mathbf{g}$ action on the particle and the surrounding fluid is expressed as

$$\mathbf{F}_g = (\rho_p - \rho)\frac{1}{6}\pi d_p^3\mathbf{g} = (\rho_p - \rho)V_p\mathbf{g} \qquad [5]$$

where ρ is the fluid density, ρ_p is the particle density, and V_p is the particle volume. The electromagnetic force acts on the object submerged in a fluid *via* the induced electric current in the particle (if it is electrically conducting) and due to the fluid pressure redistribution in the vicinity of the body in the presence of the electromagnetic field. The behavior of bodies of different shapes and electrical conductivities is considered in Reference 7. For the case of electrically nonconducting particles (oxides, carbides, *etc.*), the electromagnetic force in a gradient field can be approximated as

$$\mathbf{F}_e = -\frac{3}{2}V_p\mathbf{f}_e \qquad [6]$$

where $\mathbf{f}_e$ is the electromagnetic force in the fluid at the location of the particle.

The numerical integration of Eqs. [1] and [2] can be done for each individual particle of various properties depending on the initial seeding locations. The time-dependent force $\mathbf{F}$ is very sensitive to the location and the local slip velocity $\Delta\mathbf{u}$; therefore, the stability of the long-term integration along the particle tracks can be adversely affected by the numerical integration scheme choice. The classical integration schemes are limited to extremely small time-steps, which could make the numerical solution very difficult for the dynamic flow conditions. Therefore, we propose a new scheme based on a locally analytical solution in the vicinity of the particle location. We observe that Eq. [2] in combination with Eqs. [3] through [5] can be rewritten explicitly as

$$\partial_t\Delta\mathbf{u} + a(t)\Delta\mathbf{u} = \mathbf{b}(t)$$
$$a(t) = 3C_d^*\nu\rho\pi d_p/m_p \qquad [7]$$
$$\mathbf{b}(t) = \partial_t\mathbf{u} - (\mathbf{F}_g + \mathbf{F}_e)/m_p$$

where the new time-dependent functions $a(t)$ and $b(t)$ are introduced to facilitate the derivation of the analytical solution for the unknown slip velocity $\Delta\mathbf{u} = \mathbf{u} - \mathbf{u}_p$. The time-dependent equation set [7] can be solved analytically for $\Delta\mathbf{u}(t)$, if $a(t)$ and $\mathbf{b}(t)$ are known. This solution can be used locally at the current time-step for the functions $a(t)$ and $\mathbf{b}(t)$ available from the numerical solution of the fluid flow and the electromagnetic field at the time-step t_n, in order to advance the solution to the next time-step $t_{n+1} = t_n + \Delta t$:

$$\Delta\mathbf{u}_{n+1} = \frac{\mathbf{b}_n}{a_n} + \left[\Delta\mathbf{u}_n - \frac{\mathbf{b}_n}{a_n}\right]e^{-a_n\Delta t} \qquad [8]$$

Combining the scheme [8] for [2] and the second-order trapezoidal rule for [1], the time integration for the particle tracks is stable for the time-steps of the same size as the unsteady fluid flow solution, *i.e.*, variable steps of the order 1 ms or larger for the present problem.

B. *Drifting Concentration Model*

An alternative approach to the particle distribution predictions can be based on the multiphase flow assumption. The model assumes that the mixture of various phase components behaves as a single fluid. Each phase is represented by the species concentration

equation for the drifting particles of various properties. The advection of the particles then occurs with the drift velocity calculated from a balance of forces acting on each phase or particle type. In the simplified case, the drift velocity is assumed stationary, corresponding to the terminal particle velocity after the initial acceleration. This means that the local drift velocity for a phase can be calculated from Eq. [2] when

$$\partial_t \mathbf{u}_p = \mathbf{F}_d + \mathbf{F}_g + \mathbf{F}_e = 0 \qquad [9]$$

With the expressions [4] through [6] for the forces, we obtain the phase or particle drift velocity:

$$\mathbf{u}_p = \mathbf{u} + \frac{d_p^2}{18\nu\rho C_d^*}\left[(\rho_p - \rho)\mathbf{g} - \frac{3}{2}\mathbf{f}_e\right] \qquad [10]$$

This drift velocity then is advecting the particular phase concentration C_p according to the Eulerian transport equation

$$\partial_t C_p + \mathbf{u}_p \cdot \nabla C_p = \nabla \cdot \nu_p \nabla C_p \qquad [11]$$

assuming that there are no sources or agglomeration, and the boundary conditions correspond to the condition that the particles are not leaving the volume of the magnetically levitated fluid sample:

$$\partial_n C_p = 0 \qquad [12]$$

The concentration development problem formulated with the equations [11] and [12] was solved by the pseudo-spectral method similar to the temperature problem in Bojarevics *et al.*[8] The time advancement scheme was the second-order semi-implicit Crank–Nicolson, and the time- steps were reduced to 10^{-5} s in order to preserve the stability, particularly for the larger particles with very high drift velocities.

III. NUMERICAL PARTICLE TRACKING RESULTS

The particle tracking algorithm is intended to be compatible with the dynamically varying fluid flow with a free surface. An example of the computed flow and temperature field is shown in Figure 1 for an iron spherical sample initially of 1.8-cm diameter (left). The cold crucible wall is removed from the figure to permit a better view. However, the temperature distribution clearly shows where the surface is contacting the water-cooled wall for the initial 5 ms (blue zones). The magnetic forces, created in the skin layer of the liquid metal, push the liquid surface in- and upward, as can be seen from Figure 2. The total vertical force initially is more than sufficient to levitate completely the liquid in the crucible. After the surface deforms and undergoes a series of inertial oscillations, the shape is deformed, conforming to the electromagnetic field intensity. The electromagnetic coupling is reduced and the total force is no longer sufficient to levitate the sample. It is instead confined away from the cold crucible walls, making contact only at a very small bottom area. If the supplied current in the coil is further increased, the deformation increases and the bottom part performs oscillations attaching to and detaching from the crucible. The associated fluid flow is quite intense in the bottom region. The following simulations were performed at the lower current of 800 A at 300 kHz in order to make the flow more stable and to achieve a stationary recirculation within the confined liquid metal.

The Lagrangian tracking model can follow the particles in an arbitrary three-dimensional time varying fluid flow. Figure 3 demonstrates some particle tracks for a different coil geometry, when there is a substantial contact of the liquid to the solid wall. During the initial

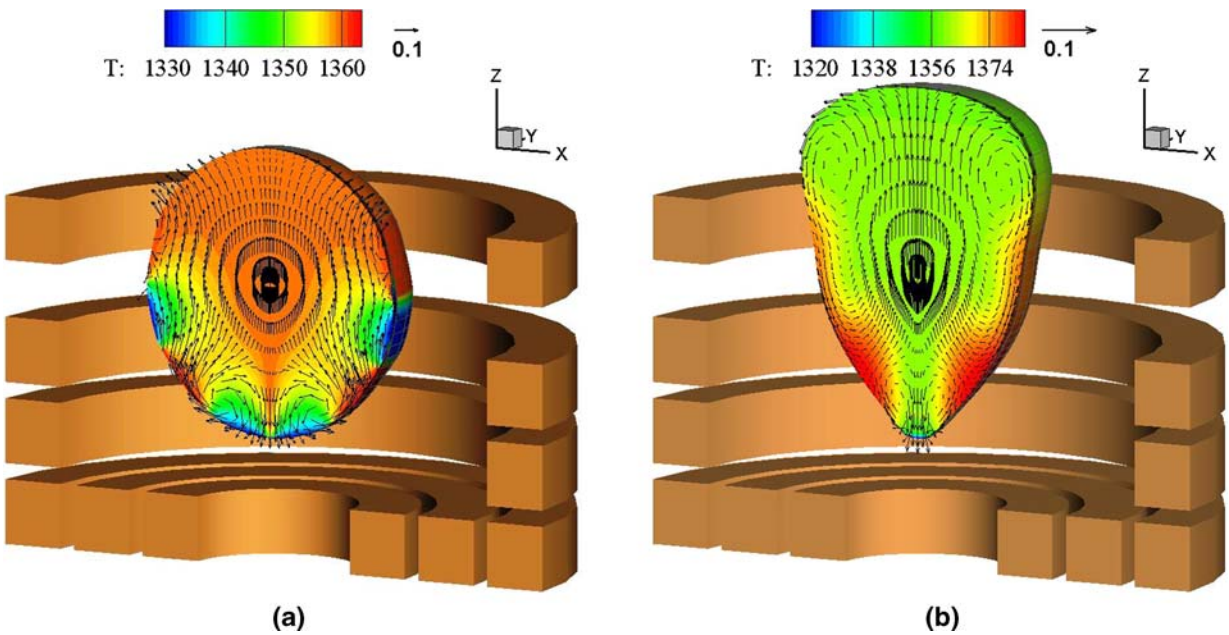

Fig. 1—Perspective view of the initial and final fluid flow and temperature for the sample partially levitated in the AC coil (shown) and the cold crucible (not shown).

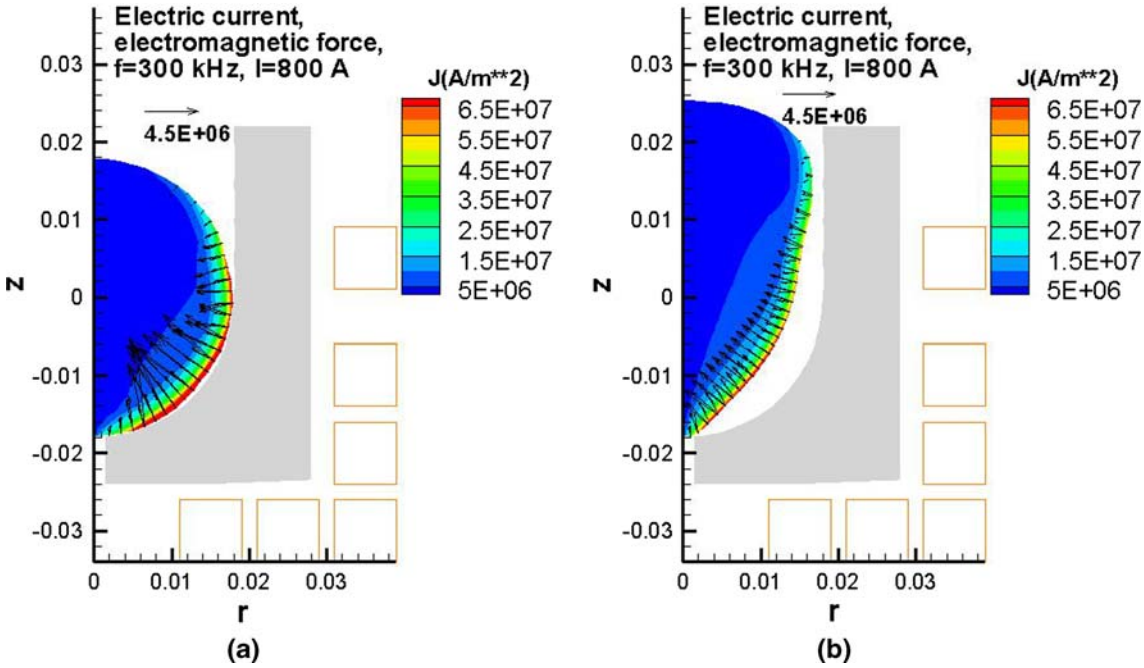

Fig. 2—Initial and final induced electric current and force distribution for the self-adjusting shape.

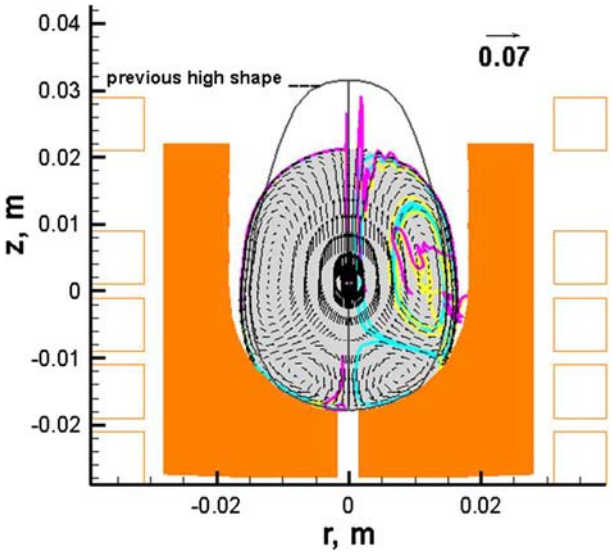

Fig. 3—Particle paths while adjusting to the electromagnetic levitation, resulting from the time-dependent variation of the fluid velocity field and the molten metal shape (shown at the final stage).

stage of the levitated sample deformation, particles follow the in- and upward motion of the fluid. At the later stage, the metal height decreases, assuming the equilibrium shape in the confining magnetic field. The paths of various size particles show their positions during this intensively oscillating stage, being partly outside the final metal shape shown in the figure.

The initial oscillating stage is very short, just about 0.3 to 0.5 seconds, after which a stationary shape is assumed with the flow exhibiting two recirculating vortices. The following systematic analysis of the particle tracking will be performed for the stationary flow stage in the fully levitated sample, after initially seeding particles of three sizes (1, 10, and 100 μm) in the metal at the equatorial plane at four different radii (right part in Figures 4 through 6) and at the central axis at four different heights (left part in the Figures 4 through 6). The particles are electrically nonconducting and their density is $\rho_p = 3000$ kg/m^3, which is less than half that of liquid iron, $\rho = 7230$ kg/m^3. As can be seen from Figure 2, the electromagnetic skin layer is very thin, and the magnetic force is effective only in the external fluid layer. The larger the particle, the larger the buoyancy and the electromagnetic force effect. For the small 1-μm particles, the fluid drag is the dominant force, and these particles follow the fluid velocity streamlines (Figure 4). The 1-μm particles are not trapped anywhere in the fluid volume and continue circulating even after a very long simulation time of 60 seconds.

The medium-sized particles of 10 μm are more sensitive to the electromagnetic expulsion force acting in the skin layer region. Initially, the particles located away from the surface are subject to the same flow drag and buoyancy as the smaller ones; therefore, the tracks are similar. However, as soon as they reach a location with significant electromagnetic force, they expel to the surface and gradually move to an equilibrium position where the forces are in balance. After about 5 seconds, all the medium-sized particles reach the stable position at a lower part of the sample surface (Figure 5).

The largest 100-μm particles experience a very significant electromagnetic interaction due to the pressure redistribution around them. In a similar time scale of about 5 seconds, all the seeded particles have reached the equilibrium position on the surface, which is higher

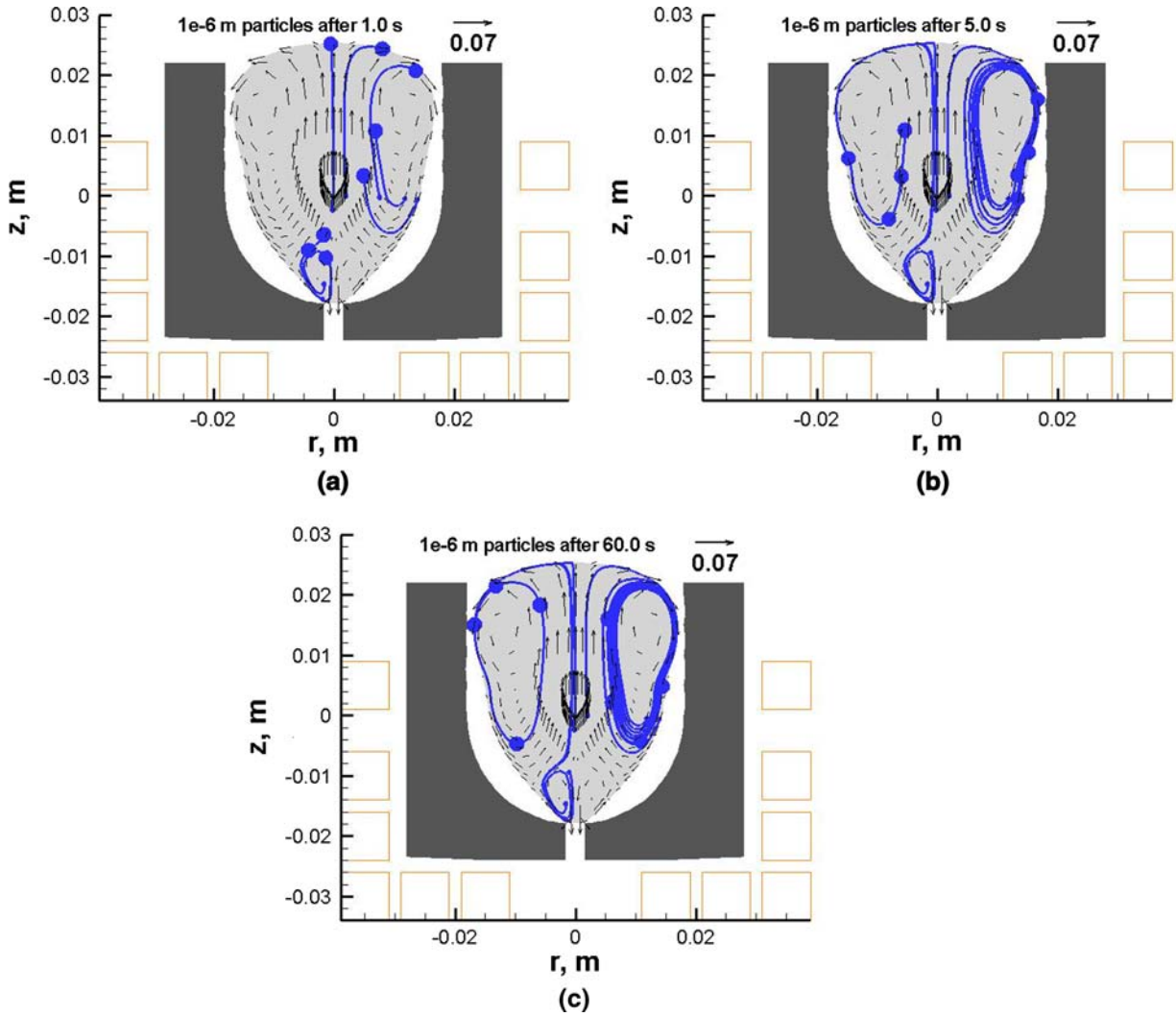

Fig. 4—Lagrangian paths at various time intervals for the 1-μm particles: no electromagnetic trapping. The large dot indicates final position, and the small, initial.

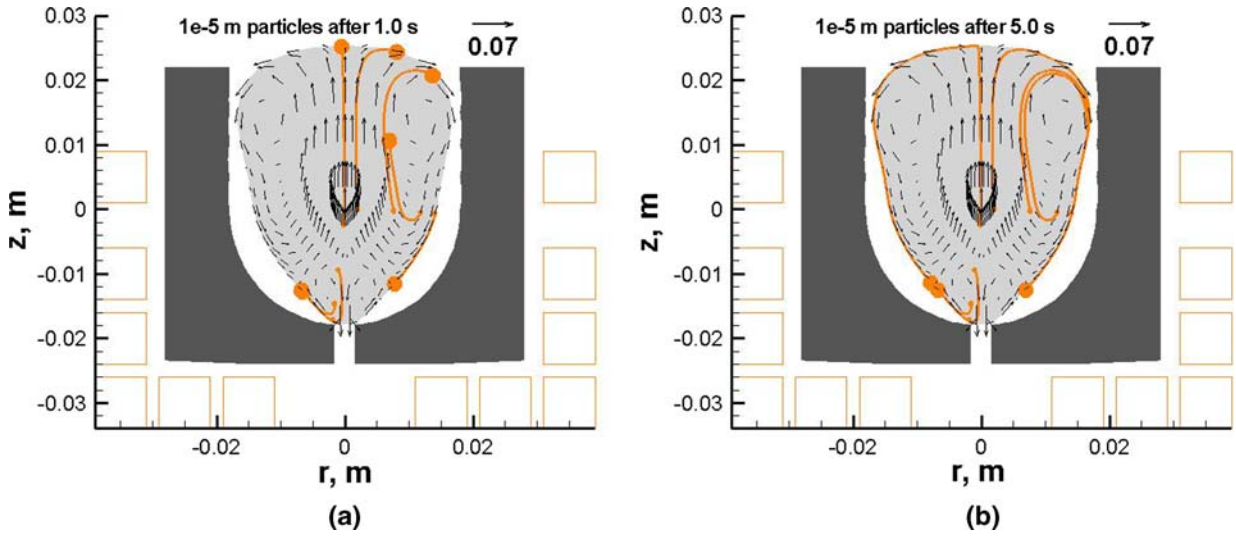

Fig. 5—Lagrangian paths after various time intervals for the 10-μm particles: finally collected at the lower position on the surface.

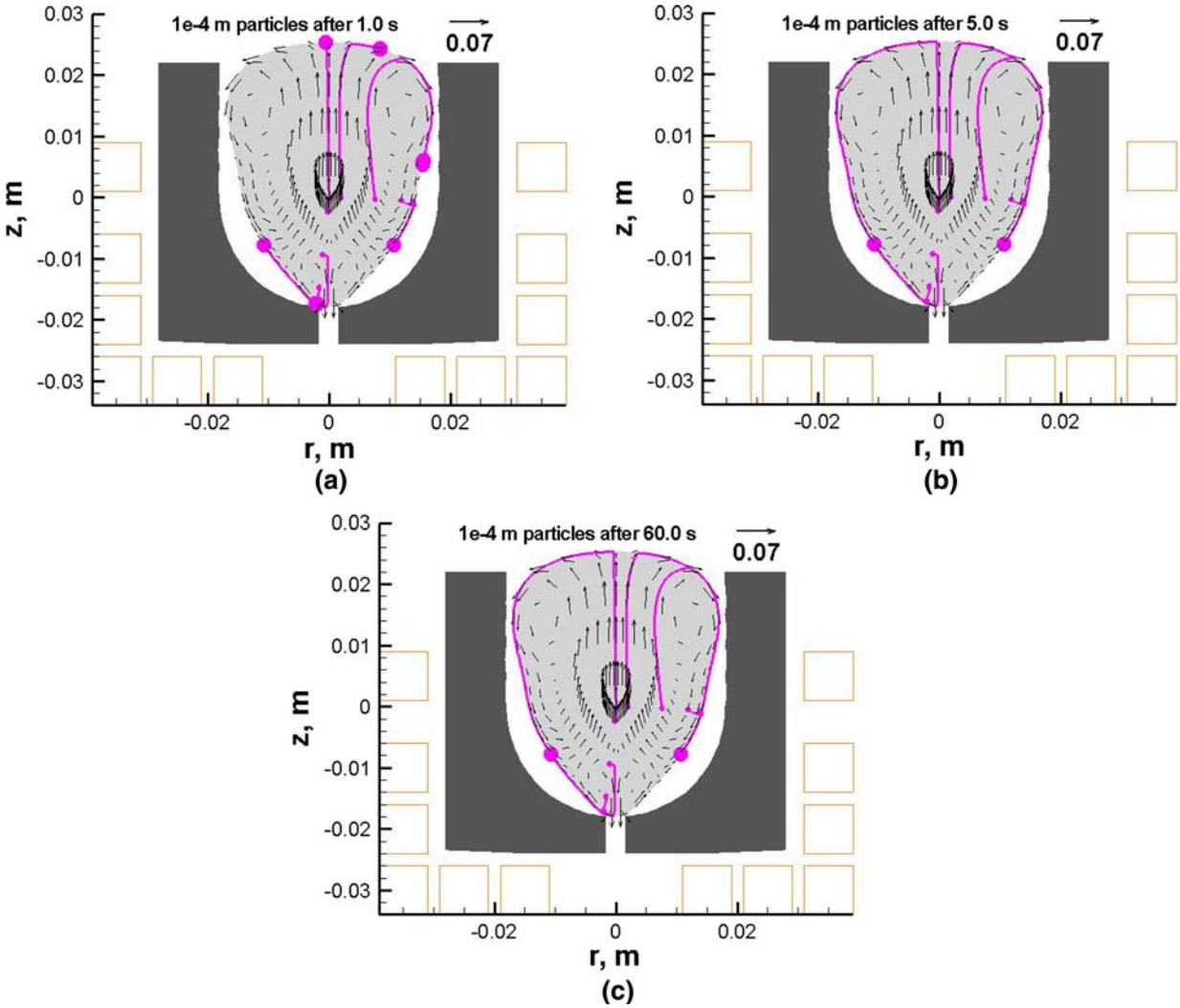

Fig. 6—Lagrangian paths after various time intervals for the 100-μm particles: the final "trapping" occurs at a higher position on the surface.

than for the medium-size particles (Figure 6). They retain this position in the turbulent flow even after the long simulation time of 60 seconds. The largest particles are the most stably separated and confined to the specific locations on the surface.

The following simulations were done, in parallel, using the Lagrangian tracking (as previously described) and the alternative particle drift concentration method. We start the particle tracking when the flow has reached a stationary state, and then introduce the initial seeding particles at the equatorial radial positions. The initial concentration C_p is zero in all the fluid volume except the equatorial nodes, where the nondimensional $C_p = 1$. This is shown in Figure 7 together with the largest 100-μm particle drift velocity representation by arrows instead of the fluid velocity (shown in all other similar pictures). The particle drift velocity $\mathbf{u}_p$ is considerably different from the fluid velocity $\mathbf{u}$. The velocity scale for the large particle drift is about two orders of magnitude larger than the fluid velocity in the region of the electromagnetic force action. Figure 7 demonstrates the fact that the drift velocity distribution does not necessarily comply with the continuity, div $\mathbf{u}_p \neq 0$, as opposed to the fluid flow velocity, div $\mathbf{u} = 0$. For this reason, the Eulerian advection equation is in the generic form [11], not in the divergence form often used.

Figure 8 illustrates the development in time of the concentration of the large particles. These particles are quickly drawn to the surface at the position coinciding with the Lagrangian particle final location. The concentration solution is affected by the turbulent diffusion term in Eq. [11] and some numerical diffusion because of the severe limitations on the time-step length. Qualitatively, both particle tracking methods give a similar final result.

The small size particle concentration exhibits significantly different behavior. Starting with the same initial distribution on the equatorial radius, the concentration of these particles dynamically follows the Lagrangian particle tracks for a significant time (Figure 9). Initially, the maximum concentration is drawn downward by the drift velocity; then, along the streamlines of the fluid

velocity, it completes one more full circulation cycle. Note, that for the smallest size particles, the drift velocity $\mathbf{u}_p$ practically coincides with the fluid velocity $\mathbf{u}$. The turbulent diffusion term in Eq. [11] is noticeable as well, which leads to the concentration spread out with the time advancement. However, qualitatively, the concentration maximum is remarkably well distributed within the Lagrangian particle recirculation loop.

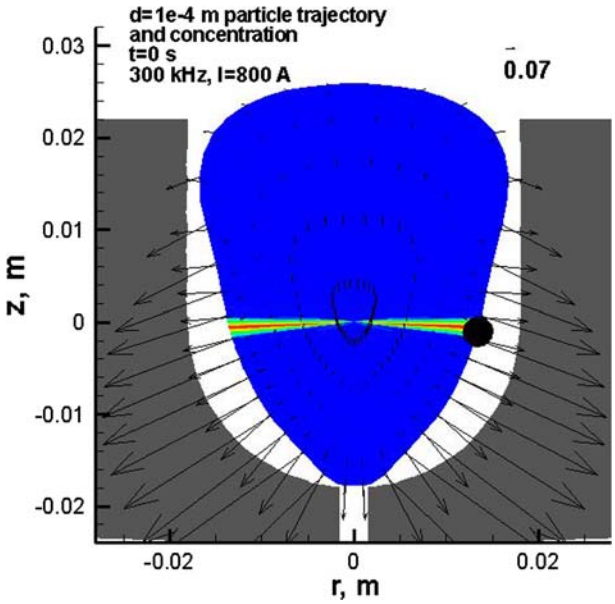

Fig. 7—Initial concentration and the particle drift velocity $\mathbf{u}_p$ (very large in the skin-layer region) for the large 100-μm particles.

IV. CONCLUSIONS AND DISCUSSION

The two particle tracking methods give very similar final results. The larger particles of the size 10 to 100 μm are easily collected in the cold crucible on the surface at the positions depending on their size. The small particles 1-μm size or less are predicted to remain in the bulk of the liquid in correspondance with the experimental observations. The Lagrangian tracking method is more flexible when used with the proposed numerical time-stepping scheme, permitting long-time integration for the time-dependent fluid flow. It is possible to represent simultaneously the various particle sizes/types, provided a transport equation is solved for each family. The big advantage of the drift flux approach is that turbulence can be included without expensive random-walk models as needed in the Lagrangian option.

Cold crucible induction melting offers a quick and cost-effective method of producing samples for the assessment of inclusion content in alloys. However, microscopic examination of the sample is made difficult due to the curved surface of the button. Therefore, it is an important step forward to be able to predict the locations of the most detrimental inclusions and speed up the analysis, through the application of this model. The model may also be scaled up to larger crucibles to predict the performance of the melting process at an industrial scale. An example where this model may be applied is in the use of bottom pouring cold crucibles, which may be used for casting ultrapure melts.[12] In this process, the metal is melted in the levitated condition; then, after a plug is removed from the crucible, the liquid is allowed to pour into a mold as the power is removed. It is hoped that inclusions on the surface of the melt will be trapped in a solid skull formed by metal

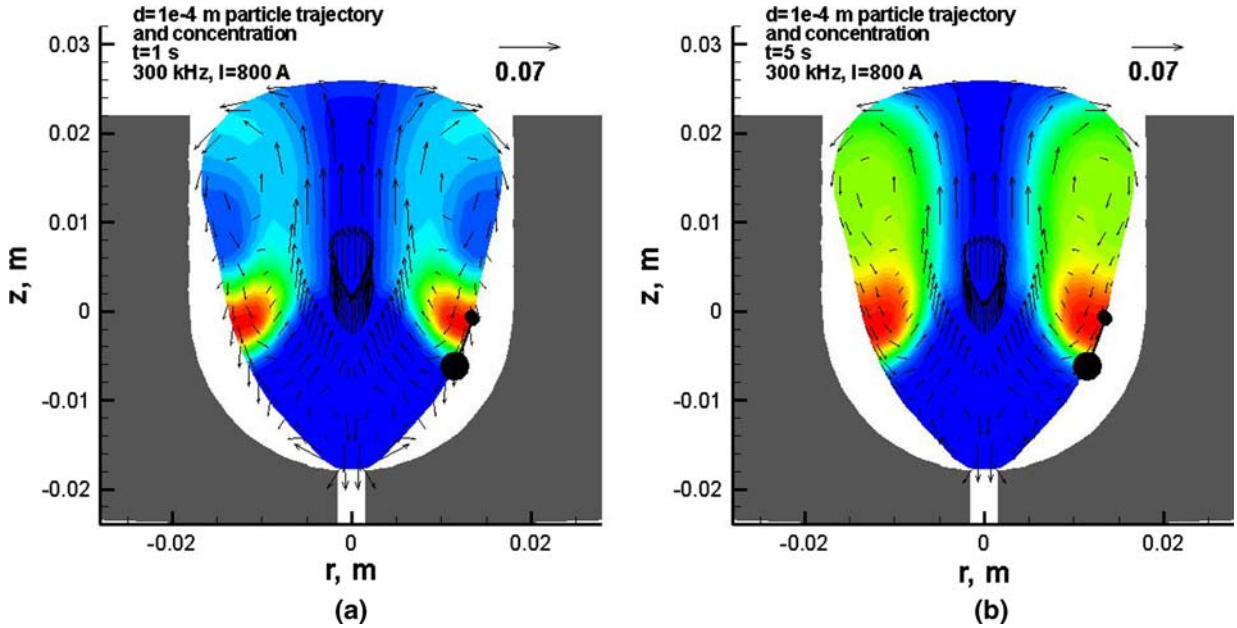

Fig. 8—Saturation of the concentration variation in time for the large 100-μm particles and the fluid flow velocity $\mathbf{u}$. A single particle track shown for comparison.

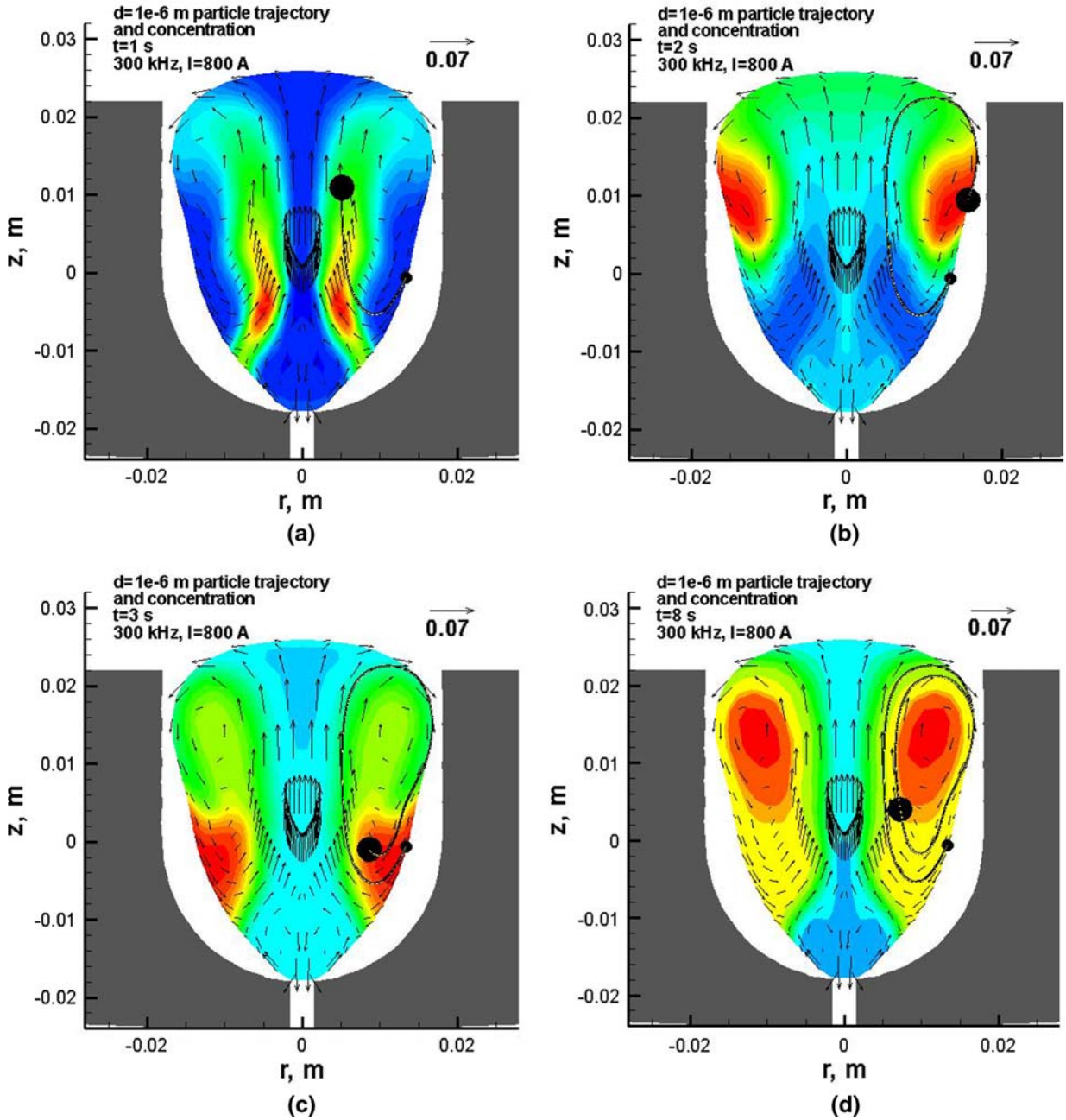

Fig. 9—The time-dependent variation of concentration for the small 1-μm particles and the particle drift velocity at 1, 2, 3, and 8 s, respectively, after the initial seeding similar to Figure 7. A single particle track is shown for comparison.

freezing against the crucible wall. This process will rely on the positions of the inclusions while the melt is levitated, and the model may be used to optimize the design to ensure the large inclusions are trapped.

REFERENCES

1. L. Barnard, R.F. Brooks, P.N. Quested, and K.C. Mills: *Ironmaking and Steelmaking*, 1993, vol. 20 (5), pp. 344–49.
2. T. Tanaka, N. Yoshida, Y. Ikenaga, and M. Horie: *Proc. 3rd Int. Symp. Electromagnetic Processing Materials*, ISIJ, Nagoya, 2000, pp. 271–76.
3. S. Taniguchi and A. Kikuchi: *Proc. 3rd Int. Symp. Electromagnetic Processing Materials*, ISIJ, Nagoya, 2000, pp. 315–20.
4. T. Toh, H. Yamamura, M. Wakoh, and E. Takeuchi: *Proc. 4th Int. Symp. Electromagnetic Processing Materials*, MADYLAM, Lyon, 2003, pp. 226–31.
5. T. Toh, H. Yamamura, H. Kondo, M. Wakoh, S. Shimasaki, and S. Taniguchi: *ISIJ Int.*, 2007, vol. 47 (11), pp. 1625–32.
6. D. Leenov and A. Kolin: *J. Chem. Phys.*, 1954, vol. 22 (4), pp. 683–88.
7. V. Bojarevics, J. Freibergs, E. Shilova, and E. Shcherbinin: *Electrically Induced Vortical Flows*, Kluwer Academic Publishers, Dordrecht, 1989, p. 248.
8. V. Bojarevics, R.A. Harding, K. Pericleous, and M. Wickins: *Metall. Mater. Trans. B*, 2004, vol. 35B, pp. 785–803.

9. R. Clift, J.R. Grace, and M.E. Weber: *Bubbles, Drops, and Particles*, Dover Publications, Mineola, NY, 2005, p. 381.
10. P.G. Tucker: *J. Fluids Eng.*, 2001, vol. 123, pp. 372–81.
11. K.A. Pericleous and S.N. Drake: *Numerical Simulation Fluid Flow Heat/Mass Transfer Processes, Lecture Notes Engineering*, Springer, Berlin, 1986, vol. 85, pp. 375–85.
12. H. Tadano, K. Kainuma, T. Take, T. Shinokura, and S. Hayashi: *Proc. 3rd Int. Symp. Electromagnetic Processing Materials*, ISIJ, Nagoya, 2000, pp. 277–82.